Optics and Lasers in Engineering 121 (2019) 11–17

Contents lists available at ScienceDirect

Optics and Lasers in Engineering

journal homepage: www.elsevier.com/locate/optlaseng

Random three-step phase retrieval approach based on difference map Gram–Schmidt orthonormalization and Lissajous ellipse fitting method

Yu Zhang [a,b,*], Xiaobo Tian [c], Rongguang Liang [c]

[a] Institute of Materials Physics, College of Science, Northeast Electric Power University, Jilin, Jilin 132012, China
[b] State Key Laboratory of Applied Optics, Changchun Institute of Optics, Fine Mechanics and Physics, Chinese Academy of Sciences, Changchun, Jilin 130022, China
[c] College of Optical Sciences, University of Arizona, Tucson, Arizona 85721, USA

ARTICLE INFO

Keywords:
Phase-shifting algorithm
Difference map Gram–Schmidt normalization
Lissajous ellipse fitting
Phase shift
Accuracy
Computational time

ABSTRACT

To achieve high measurement accuracy with less computational time in phase-shifting interferometry, a random phase retrieval approach based on difference map Gram–Schmidt othonormalization and Lissajous ellipse fitting method (DGS-LEF) is proposed, it easy to implement and only needs three phase shifted interferograms, it doesn't need pre-filtering, moreover, the phase shift can be random except for too small relative phase shift between two adjacent interferograms, last but not least, this method is effective for the symmetrical and asymmetrical fringes. The simulations and experiments verify the correctness and feasibility of DGS-LEF.

1. Introduction

Phase-shifting interferometry (PSI) has been widely used in the high precision phase measurement, such as optical surface testing and deformation measurement [1–3]. In order to obtain accurate tested phase, the outstanding phase-shifting algorithm (PSA) is essential. The accuracy of the standard PSA depends on the accuracy of the phase shift [4–6], which should be a special value (e.g. $\pi/2$), the practical phase shift is difficult to equal to the pre-set phase shift due to the phase shift error caused by the miscalibration of piezo-transducer, vibrational error, air turbulence in the working environment, instability of the laser frequency, and so on [7–9].

To overcome the phase shift error, several PSAs with random phase shift have been proposed [7–12]. In 1992, Farrell and Player [13] utilized Lissajous figures and ellipse fitting to calculate the phase difference between two interferograms. In 2004, an advanced iterative algorithm based on a least-squares iterative procedure was introduced to extract phase distribution from randomly phase shifted interferograms [14]. It copes with the limitation of the existing iterative algorithms by separating a frame-to-frame iteration from a pixel-to-pixel iteration, and provides stable convergence and accurate phase extraction. In 2008, Xu et al. [15] presented an advance iterative algorithm to extract phase distribution from randomly and spatially non-uniform phase shifted interferograms, this algorithm divides the interferograms into small blocks and retrieves local phase shifts accurately by iterations. In 2013, an iterative PSA based on the least-squares principle was developed to overcome the random piston and tilt wavefront errors generated from the phase shifter [16]. From 2011 to 2017, [17–23] proposed a series of PSAs based on principal component analysis which is an efficient technique for phase extraction by converting a set of possibly correlated variables into a set of values of uncorrelated variables, but it cannot determine the global sign of the measured phase, and it needs more than three interferograms because it need to subtract relatively accurate mean. In 2012, Vargas et al. [24] presented a two-step demodulation based on the Gram–Schmidt orthonormalization method (GS2), where the phase shift is random and can be any value inside the range $[0, 2\pi]$ except π. The main drawback is that it requires subtracting the DC term by filtering. In 2016, Liu et al. [25] proposed a PSA which can simultaneously extract the tested phase and phase shift from only two interferograms using Lissajous figure and ellipse fitting technology, but it needs pre-filtering and the non-uniform intensity distribution will affect the accuracy.

For the PSAs with less than three phase shifted interferograms, it is difficult to obtain the high accuracy and cost less time simultaneously. Generally the accuracy of the iterative algorithm is relatively high, but the computational time is also relatively long, and the computational time of the non-iterative algorithm is shorter, however, its accuracy is lower than that of the iterative algorithm. Moreover, for both the iterative and non-iterative algorithm, the pre-filtering will spend more time and affect the accuracy. Hence, to obtain the high accuracy and save time simultaneously, the research of the non-iterative three-step PSA with no pre-filtering and high accuracy is essential.

In this paper, we will discuss the accurate and timesaving phase retrieval approach with random phase shift. Section 2 presents the

* Corresponding author at: Northeast Electric Power University, Changchun Road No.169, Jilin, Jilin 132012, China.
E-mail address: 521zhangyu2008@163.com (Y. Zhang).

https://doi.org/10.1016/j.optlaseng.2019.03.012
Received 20 January 2019; Received in revised form 9 March 2019; Accepted 17 March 2019

principle and process of the proposed PSA based on difference map Gram–Schmidt othonormalization and Lissajous ellipse fitting method (DGS-LEF). In Section 3 the simulation of DGS-LEF is discussed, and the comparison with AIA is performed. Section 4 evaluates the novel PSA with the experimental data. The conclusion is finally drawn in Section 5.

2. Principles

In PSI, the intensity distribution of the phase shifted interferograms can be expressed as:

$$I_m(x,y) = a_m(x,y) + b_m(x,y)\cos\left(\varphi(x,y) + \delta_m\right) \tag{1}$$

where $m = 1,2,\ldots, M$ represents the image index with M the total number of phase shifted interferograms. M is set to 3.$a_m(x, y)$, $b_m(x, y)$ and $\varphi(x, y)$ respectively represent the background intensity, modulation amplitude and tested phase. δ_m represents the phase shift. Because there is only an invariable difference δ_1 between $\varphi(x, y)$ and $\varphi(x, y) + \delta_1$, which doesn't affect the phase distribution, for simplicity, we define $\delta_1 = 0$, and omit the subscript (x, y) in the following discussion.

Firstly, we implement the subtraction between the three phase shifted interferograms to filter the background intensity since the subtraction can cost less time than the filtering algorithm. Generally for the background intensity and modulation amplitude distributions, both the fluctuation between different interferograms and the non-uniformity between different pixels exist, however, the subtraction can still filter most of the background intensity, hence, for simplicity, we assume that a_m and b_m are irrelevant to the pixel position, only relevant to the image index in the filtering process.

Here, two difference maps between the 1st, 2nd, and 3rd interferograms can be defined as:

$$\begin{aligned} D_1 = I_1 - I_2 &= \left(b_1 + b_2\right)\sin\left(\frac{\delta_2}{2}\right)\sin\left(\varphi + \frac{\delta_2}{2}\right) \\ &\quad + \left(b_1 - b_2\right)\cos\left(\frac{\delta_2}{2}\right)\cos\left(\varphi + \frac{\delta_2}{2}\right) + a_1 - a_2 \\ D_2 = I_1 - I_3 &= \left(b_1 + b_3\right)\sin\left(\frac{\delta_3}{2}\right)\sin\left(\varphi + \frac{\delta_3}{2}\right) \\ &\quad + \left(b_1 - b_3\right)\cos\left(\frac{\delta_3}{2}\right)\cos\left(\varphi + \frac{\delta_3}{2}\right) + a_1 - a_3 \end{aligned} \tag{2}$$

Assuming that $(b_1 - b_2)$ and $(b_1 - b_3)$ approximate to zero, therefore $(b_1 - b_2)\cos(\frac{\delta_2}{2})\cos(\varphi + \frac{\delta_2}{2})$ and $(b_1 - b_3)\cos(\frac{\delta_3}{2})\cos(\varphi + \frac{\delta_3}{2})$ both close to zero. Finally we can simply the Eq. (2) as

$$\begin{aligned} D_1 &= \alpha\sin\left(\varphi + \tfrac{\delta_2}{2}\right) + a_0 = \alpha\cos\left(\Phi - \tfrac{\pi}{2}\right) + a_0 = \alpha\cos\left(\Psi\right) + a_0 \\ D_2 &= \beta\sin\left(\varphi + \tfrac{\delta_3}{2}\right) + b_0 = \beta\cos\left(\Phi + \Delta - \tfrac{\pi}{2}\right) + b_0 = \beta\cos\left(\Psi + \Delta\right) + b_0 \end{aligned} \tag{3}$$

where $\alpha = (b_1 + b_2)\sin(\frac{\delta_2}{2})$, $\beta = (b_1 + b_3)\sin(\frac{\delta_3}{2})$, $a_0 = a_1 - a_2$, $b_0 = a_1 - a_3$, $\Phi = \varphi + \frac{\delta_2}{2}$, $\Psi = \Phi - \frac{\pi}{2}$, $\Delta = \frac{\delta_3 - \delta_2}{2}$.

From Eqs. (2) and (3), we can see that the background intensity has been eliminated mostly by the simple subtraction, then we use Gram–Schmidt othonormalization process to orthonormalize the differential vectors D_1 and D_2 [24].

For orthonormalizing two vectors $\{u_1, u_2\}$, there are three simple steps. First, we take one of the vectors and normalize it:

$$\tilde{u}_1 = u_1/\|u_1\| \tag{4}$$

Then, we orthogonalize the u_2 with respect to the $\tilde{u}_1$ vector, subtracting its projection as

$$\hat{u}_2 = u_2 - \langle u_2, \tilde{u}_1\rangle \cdot \tilde{u}_1 \tag{5}$$

At last, we obtain $\tilde{u}_2$ by normalizing $\hat{u}_2$

$$\tilde{u}_2 = \hat{u}_2/\|\hat{u}_2\| \tag{6}$$

Note that, in the above equations, $\|\cdot\|$ and $\langle\cdot,\cdot\rangle$ respectively represent the 2-norm and the inner product.

According to the GS method outlined above, we orthonormalizing D_1 and D_2 as:

$$\tilde{D}_1 = \frac{D_1}{\|D_1\|} \approx \frac{\alpha\cos\left(\Psi\right) + a_0}{\kappa_1} = \frac{\alpha\cos\left(\Psi\right)}{\kappa_1} + \mathrm{X}_1 \tag{7}$$

where $\kappa_1 = \sqrt{\sum_{x=1}^{N_x}\sum_{y=1}^{N_y}(\alpha\cos(\Psi))^2}$, $\mathrm{X}_1 = \frac{a_0}{\kappa_1}$, N_x and N_y respectively correspond to the size of image columns and rows.

Then, we can obtain $\hat{D}_2$ as:

$$\begin{aligned} \hat{D}_2 &\approx \beta(\cos\left(\Psi\right)\cos\left(\Delta\right) - \sin\left(\Psi\right)\sin\left(\Delta\right)) + b_0 \\ &\quad - \left(\frac{\sum_{x=1}^{N_x}\sum_{y=1}^{N_y}\left(\alpha\beta\left(\cos^2(\Psi)\cos\left(\Delta\right) - \sin\left(\Psi\right)\cos\left(\Psi\right)\sin\left(\Delta\right)\right)\right)}{\kappa_1} + N_xN_y\mathrm{X}_1b_0\right) \\ &\quad \cdot\left(\frac{\alpha\cos\left(\Psi\right)}{\kappa_1} + \mathrm{X}_1\right) \end{aligned} \tag{8}$$

If we have more than one fringe in the interferograms, we can use the approximation

$$\left|\sum_{x=1}^{N_x}\sum_{y=1}^{N_y}\cos^2(\Psi)\cos\left(\Delta\right)\right| \gg \left|\sum_{x=1}^{N_x}\sum_{y=1}^{N_y}\sin\left(\Psi\right)\cos\left(\Psi\right)\sin\left(\Delta\right)\right| \tag{9}$$

Therefore, we can rewrite Eq. (9) as

$$\begin{aligned} \hat{D}_2 &\approx \beta(\cos\left(\Psi\right)\cos\left(\Delta\right) - \sin\left(\Psi\right)\sin\left(\Delta\right)) + b_0 \\ &\quad - \frac{\left(\sum_{x=1}^{N_x}\sum_{y=1}^{N_y}\left(\alpha^2\beta\cos^2(\Psi)\cos\left(\Delta\right)\right)\right)\cos\left(\Psi\right)}{{\kappa_1}^2} - N_xN_y{\mathrm{X}_1}^2b_0 \\ &= -\beta\sin\left(\Psi\right)\sin\left(\Delta\right) + b_0 - N_xN_y{\mathrm{X}_1}^2b_0 \end{aligned} \tag{10}$$

Finally, we obtain $\tilde{D}_2$

$$\tilde{D}_2 \approx (-\beta\sin\left(\Psi\right))/\kappa_2 - \mathrm{X}_2 \tag{11}$$

where $\kappa_2 = \sqrt{\sum_{x=1}^{N_x}\sum_{y=1}^{N_y}(\beta\sin(\Psi))^2}$, $\mathrm{X}_2 = \frac{N_xN_y{\mathrm{X}_1}^2b_0 - b_0}{\kappa_2}$.

After the GS process, we set

$$D = \tilde{D}_1,\ N = -\tilde{D}_2 \tag{12}$$

then we can obtain the expressions with the sine and cosine signals of the tested phase.

From Eqs. (7), (11) and (12), an ellipse function can be obtained

$$\frac{\left(N - x_0\right)^2}{\left(a_x\right)^2} + \frac{\left(D - y_0\right)^2}{\left(a_y\right)^2} = 1 \tag{13}$$

where $x_0 = \mathrm{X}_2, y_0 = X_1, a_x = \beta/\kappa_2, a_y = \alpha/\kappa_1$

According to Eq. (12), a general conic function can be obtained

$$\frac{N^2}{{a_x}^2} + \frac{D^2}{{a_y}^2} - 2\frac{x_0N}{{a_x}^2} - 2\frac{y_0D}{{a_y}^2} + \frac{{x_0}^2}{{a_x}^2} + \frac{{y_0}^2}{{a_y}^2} - 1 = 0 \tag{14}$$

A general conic function can be also expressed by the following second order polynomial:

$$F = ax^2 + bxy + cy^2 + dx + fy + g \tag{15}$$

For an ellipse, Eq. (15) needs to meet the conditions of $F = 0$ and $b^2 - 4ac < 0$. In the following, we will use the Lissajous ellipse fitting (LEF) method to extract the real phase. Firstly we plot an approximate ellipse with N as the x coordinate and D as the y coordinate, then the coefficients of the ellipse function can be obtained by the least squares fitting, lastly according to Eqs. (14) and (15), the semi-major amplitude

a_x, semi-minor amplitude a_y, the center offset x_0 and y_0 can be calculated as

$$a_x = \sqrt{\frac{1}{a}}, a_y = \sqrt{\frac{1}{c}}, x_0 = -\frac{d}{2a}, y_0 = -\frac{f}{2c} \tag{16}$$

After the LEF, according to Eqs. (7), (11) and (12), sin (Ψ) and cos (Ψ) can be obtained by

$$\sin(\Psi) = \frac{N - x_0}{a_x}, \cos(\Psi) = \frac{D - y_0}{a_y} \tag{17}$$

Then the tested phase can be finally determined by

$$\Psi = \arctan\left(\frac{a_y}{a_x} \cdot \frac{(N - x_0)}{(D - y_0)}\right) \tag{18}$$

Provided that there are no fluctuation between different phase shifted interferograms, Eq. (7) will be rewritten as

$$\tilde{D}_1 == \frac{b\cos(\Psi)}{\sqrt{\sum_{x=1}^{N_x}\sum_{y=1}^{N_y}(b\cos(\Psi))^2}} \tag{19}$$

Eq. (11) will be rewritten as

$$\tilde{D}_2 \approx -\frac{b\sin(\Psi)}{\sqrt{\sum_{x=1}^{N_x}\sum_{y=1}^{N_y}(b\sin(\Psi))^2}} \tag{20}$$

Then for Eq. (13), $x_0 = 0, y_0 = 0, a_x = \sqrt{\sum_{x=1}^{N_x}\sum_{y=1}^{N_y}(b\sin(\Psi))^2}, a_y = \sqrt{\sum_{x=1}^{N_x}\sum_{y=1}^{N_y}(b\cos(\Psi))^2}$.

If we have more than one fringe in the interferograms, we have $a_x \cong a_y$, then the phase retrieval function can be simplified as

$$\Psi = \arctan\left(\frac{N}{D}\right) = \arctan\left(\frac{-\tilde{D}_2}{\tilde{D}_1}\right) \tag{21}$$

The phase retrieval function doesn't include the phase shift information since the phase shift information is eliminated in the othonormalization process as shown in Eq. (6).

We know that there is only an invariable difference $\frac{\delta_2}{2} - \frac{\pi}{2}$ between φ and Ψ, which will not affect the phase distribution, hence we can use Ψ to express the tested phase distribution. Note that, because the proposed method can't calculate the practical phase φ and phase shift δ_m, the proposed method is only suitable for the whole phase distribution calculation, not suitable to obtain the displacement by subtracting the phase before deformation from that after deformation, the advanced iterative algorithm can be used to calculate the displacement [14].

3. Simulation

To show the performance of the proposed method, we perform several simulations, moreover, we compare DGS-LEF with well-evaluated advanced iterative algorithm [14], we choose the advanced iterative algorithm because it is also a random three-step PSA, and it takes the fluctuation between different interferograms and the non-uniformity between different pixels into consideration as the proposed method.

Table 1
RMS phase errors with different levels of noises using different methods (rad).

SNR(dB)	DGS-LEF	Advanced iterative algorithm
20	0.1178	0.1225
30	0.0345	0.0659
40	0.0112	0.0574
50	0.0042	0.0565
60	0.0027	0.0563
70	0.0027	0.0563
No noise	0.0027	0.0563

In the following simulations, we firstly simulate the tested phase distribution which is expressed as $\varphi = N_f\pi(x^2 + y^2)(-1 \le x \le 1, -1 \le y \le 1)$, in which $N_f = 5$ is the fringe number in the interferogram, Fig. 1(a) shows the reference phase distribution. In general, the background intensity and modulation amplitude have frame-to-frame fluctuation and pixel-to-pixel variation, hence the background intensity and modulation amplitude are set as $a_i(x, y) = N_a \exp[-0.02(x^2 + y^2)]$ and $b_i(x, y) = N_b \exp[-0.02(x^2 + y^2)]$ respectively, and N_a of the 1st, 2nd and 3rd interferograms are set as 1, 0.95 and 0.9, N_b of the 1st, 2nd and 3rd interferograms are set as 0.9, 0.85 and 0.8. The phase shifts of the three phase shifted interferograms are preset as 0 rad, 1.5 rad and 3.5 rad respectively. Since there are noises in the practical interferograms, the Gaussian noise generated by the function *awgn* in Matlab is added to the interferograms.

In the first simulation, the effects of different levels of noises were studied. Three simulated phase shifted interferograms with a signal-to-noise ratio (SNR) of 20 dB and the size of 401×401 are generated, as shown in Fig. 1(b)–(d), it can be seen that the fringes are symmetrical, and the phase distributions extracted by DGS-LEF and advanced iterative algorithm are shown in Fig. 2(a) and (b), then, the phase error distributions were calculated as shown in Fig. 2(c) and (d). Table 1 shows the RMS phase errors with different levels of noises using different methods. As can be seen from Table 1, for all levels of noises, the proposed method is more accurate than the advanced iterative algorithm. Also, when there is no noise in the interferograms, only the phase error of DGS-LEF closes to 0 since the LEF process can correct the inherent error due to the fluctuating background intensity and modulation amplitude, and the slight phase error of DGS-LEF is generated by the non-uniform background intensity, modulation amplitude and approximation error. For well-evaluated advanced iterative algorithm, when there are large numbers of the interferograms, it has high accuracy, however, when the numbers of the interferograms are relatively few, its accuracy will be affected by the background intensity, modulation amplitude and noise, because we simulate the most complex circumstance and there are only three interferograms, the accuracy of the advanced iterative algorithm is lower than that of DGS-LEF. Moreover, the processing time of DGS-LEF (1.30 s) is less than that of the advanced iterative algorithm (18.59 s),

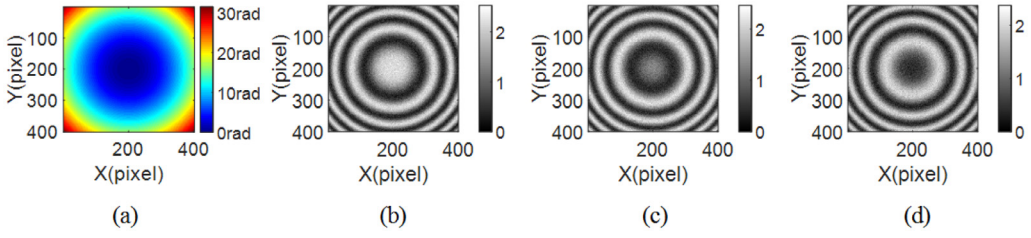

Fig. 1. Simulated phase distribution and three phase shifted interferograms with the symmetrical fringes. (a) The reference phase distribution (PV = 31.416 rad, RMS = 6.656 rad), (b), (c) and (d) three phase shifted interferograms.

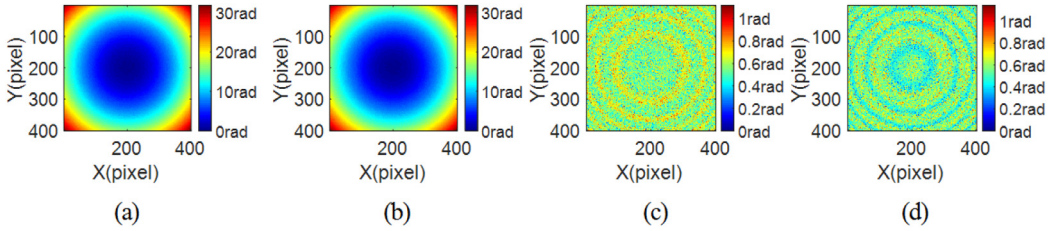

Fig. 2. Simulated results of the symmetrical fringes. (a) and (b) the phase distributions extracted by DGS-LEF (PV=31.851 rad, RMS=6.662 rad) and advanced iterative algorithm (PV = 31.845 rad, RMS = 6.663 rad), (c) and (d) the phase error distributions after using DGS-LEF and advanced iterative algorithm.

Table 2
RMS phase and RMS phase errors with different fringe numbers using DGS-LEF.

Fringes numbers	0.5	0.6	0.7	0.8	0.9	1.0	1.1	1.2
RMS phase (rad)	0.6656	0.7987	0.9319	1.0650	1.1981	1.3312	1.4643	1.5975
RMS phase error (rad)	0.1964	0.1502	0.1266	0.1193	0.1195	0.1215	0.1249	0.1272
Fringes numbers	1.3	1.4	1.5	1.6	1.7	1.8	1.9	2.0
RMS phase (rad)	1.7306	1.8637	1.9968	2.1300	2.2631	2.3962	2.5293	2.6625
RMS phase error (rad)	0.1285	0.1275	0.1249	0.1222	0.1201	0.1189	0.1187	0.1187
Fringes numbers	3.0	4.0	5.0	15	25	35	45	
RMS phase (rad)	3.9937	5.3249	6.6561	19.9684	33.2807	46.5929	59.9052	
RMS phase error (rad)	0.1181	0.1177	0.1177	0.1177	0.1178	0.1174	0.1178	

Table 3
$|\sum_{x=1}^{N_x}\sum_{y=1}^{N_y}\cos^2(\Psi)\cos(\Delta)|$, $|\sum_{x=1}^{N_x}\sum_{y=1}^{N_y}\sin(\Psi)\cos(\Psi)\sin(\Delta)|$ and their ratios with different fringe numbers using DGS-LEF.

Fringes numbers	0.5	0.6	0.7	0.8	0.9	1.0
$\lvert\sum_{x=1}^{N_x}\sum_{y=1}^{N_y}\cos^2(\Psi)\cos(\Delta)\rvert$	2.216×10^7	1.774×10^7	1.415×10^7	1.160×10^7	9.752×10^6	8.173×10^6
$\lvert\sum_{x=1}^{N_x}\sum_{y=1}^{N_y}\sin(\Psi)\cos(\Psi)\sin(\Delta)\rvert$	6.061×10^3	7.082×10^3	4.586×10^3	1.632×10^3	7.349×10^2	2.507×10^3
Ratio	3.655×10^3	2.505×10^3	3.085×10^3	7.106×10^3	1.327×10^4	3.260×10^3
Fringes numbers	1.1	1.2	1.3	1.4	1.5	1.6
$\lvert\sum_{x=1}^{N_x}\sum_{y=1}^{N_y}\cos^2(\Psi)\cos(\Delta)\rvert$	6.644×10^6	5.190×10^6	3.938×10^6	2.977×10^6	2.3143×10^6	1.909×10^6
$\lvert\sum_{x=1}^{N_x}\sum_{y=1}^{N_y}\sin(\Psi)\cos(\Psi)\sin(\Delta)\rvert$	3.520×10^3	3.357×10^3	2.015×10^3	2.069×10^2	1.122×10^3	1.499×10^3
Ratio	1.887×10^3	1.546×10^3	1.955×10^3	1.439×10^4	2.062×10^3	1.273×10^3
Fringes numbers	1.7	1.8	1.9	2.0	3.0	4.0
$\lvert\sum_{x=1}^{N_x}\sum_{y=1}^{N_y}\cos^2(\Psi)\cos(\Delta)\rvert$	1.705×10^6	1.659×10^6	1.736×10^6	1.907×10^6	2.101×10^6	1.008×10^6
$\lvert\sum_{x=1}^{N_x}\sum_{y=1}^{N_y}\sin(\Psi)\cos(\Psi)\sin(\Delta)\rvert$	1.094×10^3	3.467×10^2	4.319×10^2	1.089×10^3	6.642×10^2	4.686×10^2
Ratio	1.558×10^3	4.784×10^3	4.020×10^3	1.751×10^3	3.163×10^3	2.151×10^3
Fringes numbers	5.0	15	25	35	45	
$\lvert\sum_{x=1}^{N_x}\sum_{y=1}^{N_y}\cos^2(\Psi)\cos(\Delta)\rvert$	1.156×10^6	3.362×10^5	1.920×10^5	1.330×10^5	1.011×10^5	
$\lvert\sum_{x=1}^{N_x}\sum_{y=1}^{N_y}\sin(\Psi)\cos(\Psi)\sin(\Delta)\rvert$	3.585×10^2	1.008×10^2	57.25	39.17	28.86	
Ratio	3.224×10^3	3.334×10^3	3.354×10^3	3.396×10^3	3.503×10^3	

the advanced iterative algorithm needs more processing time because it needs several iterations.

Since we use many approximations in the proposed method, and we assume that there is more than one fringe pattern in the interferogram, in the following simulation, we vary the fringe number while fixing the SNR of noise to 20 dB to obtain the best range of fringe numbers using DGS-LEF. As can be seen from Table 2, when the fringe number is less than 0.8, the ratio of the RMS phase to the RMS phase error is less than 10 (Generally, the ratio is more than 10 in the highly accurate measurement). When the range of fringe numbers is between 0.9 and 1.2, the RMS phase error is unstable. For the range between 1.3 and 2.0, the ratio is increasing with the increase of the fringe number, and the RMS phase error is decreasing simultaneously. When the fringe numbers are more than 3, the RMS phase errors are similar. Moreover, to verify the validity of the approximation from Eq. (9), we respectively calculate $|\sum_{x=1}^{N_x}\sum_{y=1}^{N_y}\cos^2(\Psi)\cos(\Delta)|$, $|\sum_{x=1}^{N_x}\sum_{y=1}^{N_y}\sin(\Psi)\cos(\Psi)\sin(\Delta)|$ and their ratios with the different fringe numbers as shown in Table 3, we can see that, the approximation can be recognized effective for all the range of fringe numbers, and when the fringe numbers are more than 3, the ratios are

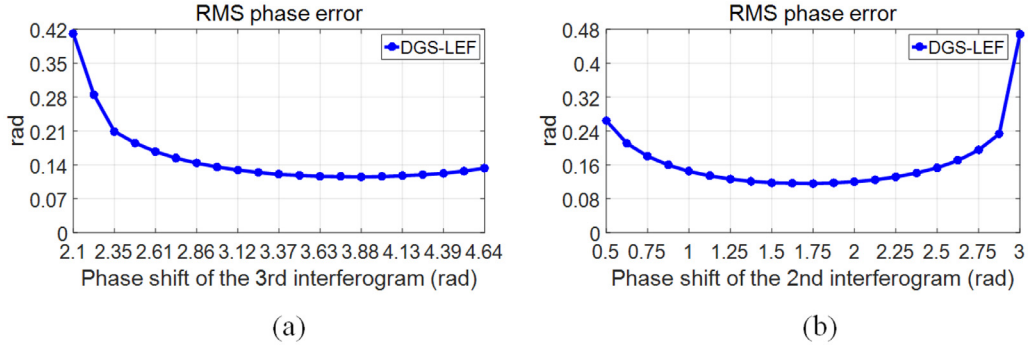

Fig. 3. The RMS phase errors of DGS-LEF using different phase shifts. (a) and (b) the relationships between the RMS phase errors and different phase shifts of the 3rd and 2nd interferograms.

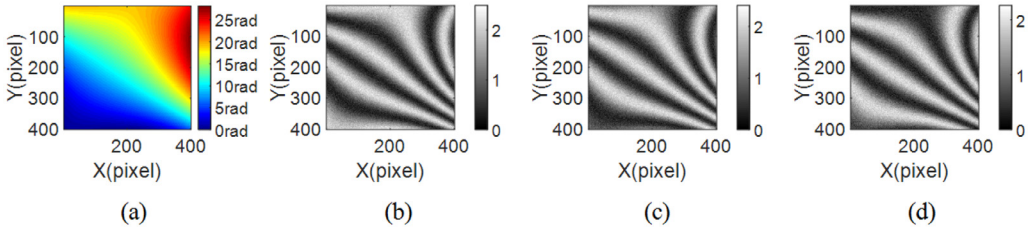

Fig. 4. Simulated phase distribution and three phase shifted interferograms with the asymmetrical fringes. (a) The reference phase distribution (PV = 28.162 rad, RMS = 7.005 rad), (b), (c) and (d) three phase shifted interferograms.

similar, in this case, the approximation error is nearly stable. Hence, we can get the same conclusion from Tables 2 and 3, the fringe numbers are best to be more than 3 if the high accuracy is requested.

We all know that the phase shift is important to the PSAs, it is necessary to discuss the RMS phase errors of DGS-LEF with different phase shifts. Firstly, the phase shifts of the 1st and 2nd frames are respectively set as 0 rad and 1.5 rad while the phase shift of the 3rd frame is uniformly changed from 2.1 rad to 4.64 rad, that is to say, the range of relative phase shift between the 2nd and 3rd frames are between 0.6 rad and π rad. Secondly, the phase shifts of the 1st and 3rd frames are respectively set as 0 rad and 3.5 rad while the phase shift of the 2nd frame is uniformly changed from 0.5 rad to 3.0 rad, that is to say, the range of relative phase shift between the 2nd and 3rd frames are between 0.5 rad and 3 rad. We can't choose too small relative phase shift between two adjacent frames because the phase error is too large for most PSAs in this situation. Other simulated conditions are same as the first simulation with 20 dB noise. As shown in Fig. 3, the relationships between the RMS phase errors and different phase shifts of the 3rd and 2nd interferograms are presented, from Fig. 3, we can see that the RMS phase errors are relatively stable and less than 0.14 rad when the phase shift of the 3rd interferogram is between 2.86 rad and 4.64 rad and when the phase shift of the 2nd interferogram is between 1.25 rad and 2.25 rad, moreover, the phase error will be relatively large when the relative phase shift between two adjacent frames is relatively small, hence, if high accuracy is required, the relative phase shift is best not to be too small.

To verify the robustness of DGS-LEF, we simulated the asymmetrical fringes and compare the proposed method with AIA. The tested phase distribution is set as

$$\varphi = 2.5\pi x - 3\pi y + \pi\left(x^2 - y^2\right) + 0.8\pi\left(x^3 - 3xy^2\right)\ (-1 \le x \le 1, -1 \le y \le 1) \tag{22}$$

Other conditions are same as the first simulation with 20 dB noise. The reference phase distribution is shown in Fig. 4(a), and Fig. 4(b)–4(d) show the three phase shifted interferograms, it can be seen that the fringes are asymmetrical. The extracted phase distributions using DGS-LEF (Fig. 5(a)) and advanced iterative algorithm (Fig. 5(b)) are similar to the reference phase distribution, that is to say, these two methods are both effective for the asymmetrical fringes, and the phase error distributions of DGS-LEF and advanced iterative algorithm are shown in Fig. 5(c) and 5(d), the RMS values are respectively 0.1176 rad and 0.1228 rad, we can see that the accuracy of DGS-LEF is also higher than that of AIA for the asymmetrical fringes. In addition, the computational time of DGS-LEF (1.29 s) is also less than that of advanced iterative algorithm (18.39 s).

Based on the above different simulations, the conclusions of the proposed DGS-LEF can be summarized as: 1) It can obtain the high accuracy with less computational time and no pre-filtering by only three phase shifted interferograms; 2) the fringe numbers are best to be more than 3 if the high accuracy is requested; 3) the phase shift can be random except for too small relative phase shift between two adjacent interferograms; 4) whether the symmetrical and asymmetrical fringes, the proposed method is valid.

4. Demonstration with experimental data

Optical experiments have been carried out to investigate the effectiveness and outstanding performance of the proposed method. Firstly, four phase shifted interferograms with the symmetrical fringes are collected to perform the phase retrieval by DGS-LEF, advanced iterative algorithm and standard 4-step PSA, the size of the interferograms is 401×401, and the phase shifts are 0, $\pi/2$, π and $3\pi/2$ respectively. The phase extracted by standard 4-step PSA is set as the reference phase due to its high accuracy. One of the interferograms is shown in Fig. 6(a), and (b) shows the reference phase distribution, the phase distributions extracted by DGS-LEF and AIA are plotted in Fig. 6(c) and (d). The differences between the reference phase and the phase obtained by DGS-LEF and AIA are shown in Fig. 6(e) and 6(f), and the RMS values are respectively 0.0374 rad and 0.0380 rad, further indicating that the accuracy of DGS-LEF is higher than that of the advanced iterative algorithm. Moreover, the computational time of DGS-LEF (1.30 s) is less than that of the advanced iterative algorithm (18.63 s).

Then, the phase shifted interferograms with the asymmetrical fringes are also collected, and the comparison for DGS-LEF and advanced itera-

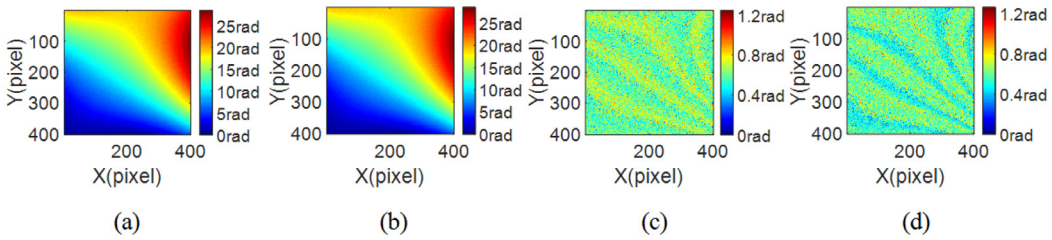

Fig. 5. Simulated results of the asymmetrical fringes. (a) and (b) the phase distributions extracted by DGS-LEF (PV=28.575 rad, RMS=7.011 rad) and advanced iterative algorithm (PV = 28.571 rad, RMS = 7.014 rad), (c) and (d) the phase error distributions after using DGS-LEF and advanced iterative algorithm.

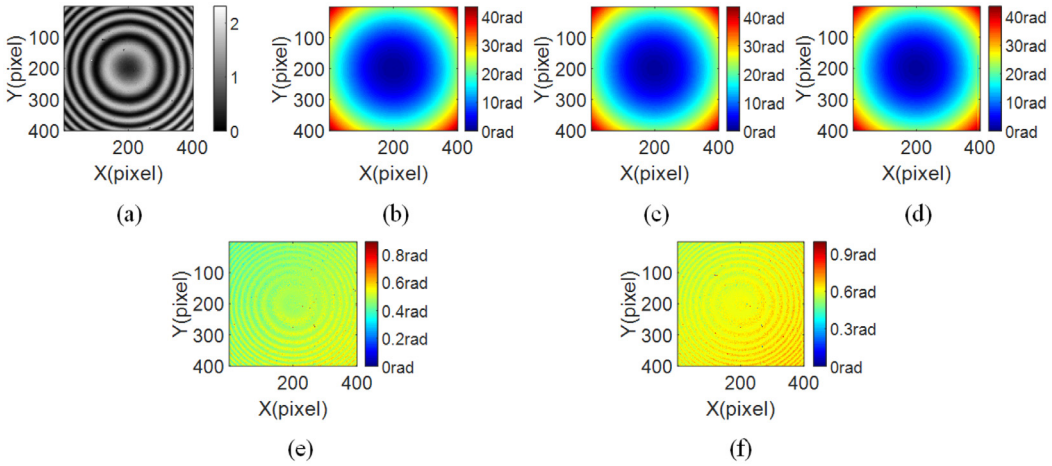

Fig. 6. Experimental results of the symmetrical fringes. (a) One of the phase shifted interferograms, (b) the reference phase distribution obtained by 4-step PSA (PV = 43.471 rad, RMS=8.933 rad), (c) and (d) the extracted phase distributions obtained by DGS-LEF (PV = 43.669 rad, RMS = 8.923 rad) and advanced iterative algorithm (PV = 43.660 rad, RMS = 8.923 rad), (e) and (f) the differences between the reference and extracted phase distributions by DGS-LEF and advanced iterative algorithm.

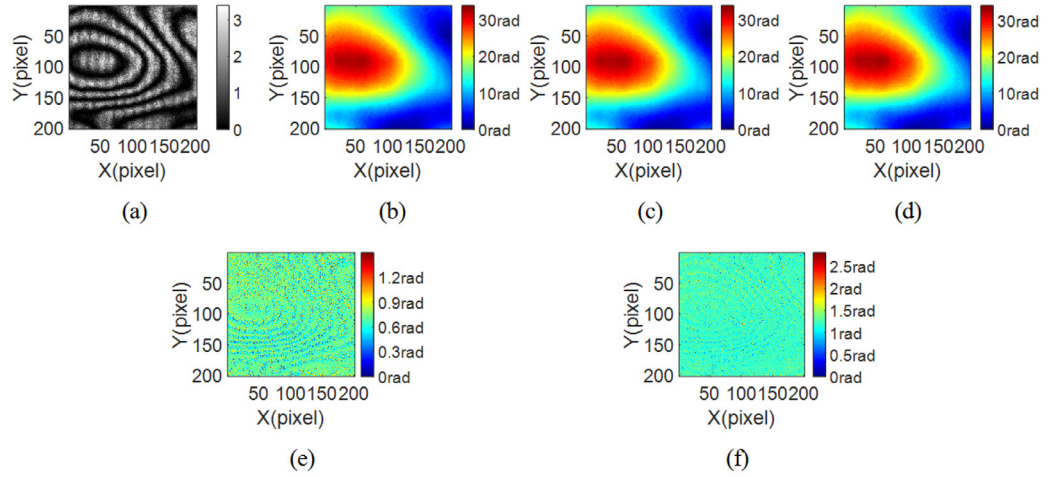

Fig. 7. Experimental results of the asymmetrical fringes. (a) One of the phase shifted interferograms, (b) the reference phase distribution obtained by 4-step PSA (PV = 33.956 rad, RMS = 8.879 rad), (c) and (d) the extracted phase distributions obtained by DGS-LEF (PV = 34.156 rad, RMS = 8.885 rad) and advanced iterative algorithm (PV = 34.133 rad, RMS = 8.885 rad), (e) and (f) the differences between the reference and extracted phase distributions by DGS-LEF and AIA.

tive algorithm are performed as the symmetrical fringes. The size of the interferograms with the asymmetrical fringes is 201 × 201, and other conditions are same as the symmetrical fringes. Fig. 7 shows the results of the asymmetrical fringes, we can see that, both DGS-LEF and advanced iterative algorithm are effective for the asymmetrical fringes, and the RMS values of the differences between the reference phase and the phase extracted by DGS-LEF and advanced iterative algorithm are 0.1461 rad and 0.1497 rad, that is to say, the accuracy of DGS-LEF is also higher than that of advanced iterative algorithm for the asymmetrical fringes. Moreover, the computational time of DGS-LEF and advanced iterative algorithm are respectively 0.98 s and 5.66 s, we can get the conclusion the same as the symmetrical fringes. Through the above experiments, we verify that, for both the symmetrical and asymmetrical fringes, the proposed DGS-LEF without pre-filtering can obtain relatively accurate result with less computational time by only three interferograms.

5. Conclusion

In this paper, we present random PSA based on difference map Gram–Schmidt othonormalization and Lissajous ellipse fitting method, the difference maps are obtained by the three phase shifted interferograms firstly, then the expressions with the sine and cosine signals of the tested phase are obtained by the GS method, finally the phase distribution is extracted by the LEF method. We have compared this proposed method with well-evaluated advanced iterative algorithm by the simulated and experimental data, we get the conclusion that the proposed method is easy to implement and can achieve high accuracy with no pre-filtering and less computational time, and the fringe numbers are best to be more than 3 if the high accuracy is requested. Moreover, the phase shift can be random except for too small relative phase shift between two adjacent interferograms. Finally, the proposed method is suitable for the whole phase distribution calculation, and effective for the symmetrical and asymmetrical fringes. The simulations and experiments demonstrate the validity of the proposed method. In summary, this proposed method is a power tool for the phase retrieval with random phase shift.

Funding

This work was supported by the National Natural Science Foundation of China (NSFC) (11304034); Project of Jilin Province Science and Technology Development Plan (20190701018GH); Program of Jilin Provincial Educational Department (JJKH20190691KJ); State Key Laboratory of Applied Optics.

References

[1] Malacara D. Optical shop testing. 3rd ed. John Wiley & Sons, Inc; 2007. Chap 1–7.
[2] Bruning JH, Herriott DR, Gallagher JE, Rosenfeld DP, White AD, Brangaccio DJ. Digital wavefront measuring interferometer for testing optical surfaces and lenses. Appl Opt 1974;13(11):2693–703. https://doi.org/10.1364/AO.13.002693.
[3] Tian C, Liu S. Two-frame phase-shifting interferometry for testing optical surfaces. Opt Express 2016;24(16):18695–708. https://doi.org/10.1364/OE.24.018695.
[4] Kinnstaetter K, Lohmann AW, Schwider J, Streibl N. Accuracy of phase shifting interferometry. Appl Opt 1988;27(24):5082–9. http://doi:10.1364/ao.27.005082.
[5] Hibino K, Oreb BF, Farrant DI, Larkin KG. Phase-shifting algorithms for nonlinear and spatially nonuniform phase shifts. J Opt Soc Am A 1997;14(4):918–30. http://doi:10.1364/josaa.14.000918.
[6] Servin M, Estrada JC, Quiroga JA. The general theory of phase shifting algorithms. Opt Express 2009;17(24):21867–81. https://doi:10.1364/oe.17.021867.
[7] Malacara D. Optical shop testing. 3rd ed. John Wiley & Sons, Inc; 2007. Chap 14.
[8] de Groot PJ. Vibration in phase-shifting interferometry. J Opt Soc Am A 1995;12(2):354–65. https://doi.org/10.1364/JOSAA.12.000354.
[9] Deck LL. Suppressing phase errors from vibration in phase-shifting interferometry. Appl Opt 2009;48(20):3948–60. https://doi.org/10.1364/AO.48.003948.
[10] Farrell CT, Player MA. Phase-step insensitive algorithms for phase-shifting interferometry. Meas Sci Technol 1994;5:648–52. https://doi:10.1088/0957-0233/5/6/003.
[11] Xu Y, Wang Y, Ji Y, Han H, Jin W. Three-frame generalized phase-shifting interferometry by a Euclidean matrix norm algorithm. Opt Laser Eng 2016;84:89–95. https://doi:10.1016/j.optlaseng.2016.04.011.
[12] Zhang Y, Tian X, Liang R. Fringe-print-through error analysis and correction in snapshot phase-shifting interference microscope. Opt Express 2016;25(22):26554–66. http://doi:10.1364/oe.25.026554.
[13] Farrell CT, Player MA. Phase step measurement and variable step algorithms in phase-shifting interferometry. Meas Sci Technol 1992;3:953–8. http://doi.org/10.1088/0957-0233/3/10/003.
[14] Wang Z. Advanced iterative algorithm for phase extraction of randomly phase-shifted interferograms. Opt Lett 2004;29(14):1671–3. https://doi.org/10.1364/OL.29.001671.
[15] Xu J, Xu Q, Chai L. Iterative algorithm for phase extraction from interferograms with random and spatially nonuniform phase shifts. Appl Opt 2008;47(3):480–5. https://doi.org/10.1364/AO.47.000480.
[16] Chen Y-C, Lin P-C, Lee C-M, Liang C-W. Iterative phase-shifting algorithm immune to random phase shifts and tilts. Appl Opt 2013;52(14):3381–6. https://doi.org/10.1364/AO.52.003381.
[17] Vargas J, Quiroga J, Belenguer T. Phase-shifting interferometry based on principal component analysis. Opt Lett 2011;36(8):1326–8. https://doi.org/10.1364/OL.36.001326.
[18] Vargas J, Quiroga J, Belenguer T. Analysis of the principle component algorithm in phase-shifting interferometry. Opt Lett 2011;36(12):2215–17. https://doi.org/10.1364/OL.36.002215.
[19] Deng J, Wang K, Wu D, Lv X, Li C, Hao J, Qin J, Chen W. Advanced principal component analysis method for phase reconstruction. Opt Express 2015;23(9):12222–31. https://doi.org/10.1364/OE.23.012222.
[20] Xu J, Jin W, Chai L, Xu Q. Phase extraction from randomly phase-shifted interferograms by combining principal component analysis and least squares method. Opt. Express 2011;19(21):20483–92. https://doi.org/10.1364/OE.19.020483.
[21] Yatabe K, Ishikawa K, Oikawa Y. Improving principal component analysis based phase extraction method for phase-shifting interferometry by integrating spatial information. Opt Express 2016;24(20):22881–91. https://doi.org/10.1364/OE.24.022881.
[22] Yatabe K, Ishikawa K, Oikawa Y. Simple, flexible and accurate phase retrieval method for generalized phase-shifting interferometry. J Opt Soc Am A 2017;34(1):87–96. https://doi.org/10.1364/JOSAA.34.000087.
[23] Yatabe K, Ishikawa K, Oikawa Y. Hyper ellipse fitting in subspace method for phase-shifting interferometry: practical implementation with automatic pixel selection. Opt Express 2017;25(23):29401–16. https://doi.org/10.1364/OE.25.029401.
[24] Vargas J, Quiroga J, Sorzano C, Estrada J, Carazo J. Two-step demodulation based on the Gram-Schmidt orthonormalization method. Opt Lett 2012;37(3):443–5. https://doi.org/10.1364/OL.37.000443.
[25] Liu F, Wang J, Wu Y, Wu F, Trusiak M, Patorski K, Wan Y, Chen Q, Hou X. Simultaneous extraction of phase and phase shift from two interferograms using Lissajous figure and ellipse fitting technology with Hilbert-Huang prefiltering. J Optics-UK 2016;18:105604. http://doi:10.1088/2040-8978/18/10/105604.